Available online at www.sciencedirect.com
ScienceDirect
Journal of Power Sources 162 (2006) 1329–1335
JOURNAL OF POWER SOURCES
www.elsevier.com/locate/jpowsour

In situ XAFS and micro-XAFS studies on $LiNi_{0.8}Co_{0.15}Al_{0.05}O_2$ cathode material for lithium-ion batteries

T. Nonaka [a,*], C. Okuda [a], Y. Seno [a], H. Nakano [a], K. Koumoto [b], Y. Ukyo [a]

[a] *Toyota Central R&D Labs., Inc., Nagakute, Aichi 480-1192, Japan*
[b] *Nagoya University, Graduate School of Engineering, Nagoya, Aichi 464-8603, Japan*

Received 29 June 2006; received in revised form 11 September 2006; accepted 12 September 2006
Available online 11 October 2006

Abstract

We have applied in situ X-ray absorption fine structure (XAFS) and in situ micro-XAFS techniques to study $LiNi_{0.8}Co_{0.15}Al_{0.05}O_2$ cathode materials in Li-ion coin cells that show various levels of capacity fading: fresh cell, cycle tested cell and aging tested cell. The change in the oxidation state and local structure of Ni and Co during charge has been investigated. Ni and Co K-edge X-ray absorption near edge structure (XANES) show that the Ni oxidation state is converted from Ni^{3+} to Ni^{4+} upon charging, whereas the Co oxidation state hardly changes. Ni K-edge extended X-ray absorption fine structure (EXAFS) reveals that the Jahn–Teller distorted NiO_6 octahedron turns into the symmetric octahedron upon charging, which is consistent with the change in the Ni oxidation state. Ni K-edge micro-XANES show that the oxidation of Ni proceeds homogeneously in a grain of $LiNi_{0.8}Co_{0.15}Al_{0.05}O_2$ within the special resolution of ~2 μm, and proceeds independently of the grain size. All the behaviors of Ni and Co observed in these experiments for the fresh cell remain unchanged after the capacity fade is induced by cycle tests or aging tests, which demonstrates the considerable stability of the $LiNi_{0.8}Co_{0.15}Al_{0.05}O_2$ cathode material.

Keywords: Li-ion battery; Nickel oxides; X-ray absorption spectroscopy; Microscopy

1. Introduction

Layer-structured transition metal oxides have been studied extensively as cathode materials for lithium-ion batteries [1]. As a substitute for widely used $LiCoO_2$, $LiNiO_2$ and its derivatives have aroused continuous interest in recent years [2]. $LiNiO_2$ is superior to $LiCoO_2$ in its lower cost and higher specific capacity [3]; however, it suffers from poor cycling reversibility and thermal instability, which prevents practical uses. More recently, $LiNi_{0.8}Co_{0.15}Al_{0.05}O_2$ is being considered as a promising cathode material because of its improved stability and electrochemical performance brought by Co and Al substitutions for Ni in $LiNiO_2$ [4–8]. Since the radii of Co^{3+} and Al^{3+} are smaller than that of Ni^{3+}, the substitutions of these ions result in shrinkage of the *a*-axis, which is considered to be an origin of stabilizing the layered structure [8]. $LiNi_{0.8}Co_{0.15}Al_{0.05}O_2$ remains as a single rhombohedral phase during charge/discharge cycling, allowing a high cycling reversibility. In spite of such improvements, $LiNi_{0.8}Co_{0.15}Al_{0.05}O_2$ still has the problem of deteriorations such as capacity fading and the increase in impedance [9]. These deteriorations occur during use (i.e., on electrochemical cycling) and/or on storage at high temperatures, being one of the most crucial problems which should be overcome for applications requiring a very long life, such as electric vehicles, satellites and standby batteries. The mechanism of deteriorations is considered to be quite complicated since Li-ion batteries consist of a number of elements such as cathode, anode, electrolyte, separator and charge collector. However, we have found that, in the case of the battery using $LiNi_{0.8}Co_{0.15}Al_{0.05}O_2$, the increase in impedance is predominantly attributed to the cathode [9].

In this study, we focused on the cathode material and investigated the changes in the oxidation state and local structure of Ni and Co during charge/discharge cycling using in situ Ni and Co K-edge X-ray absorption fine-structure spectroscopy (XAFS). In situ XAFS is a powerful tool to provide an understanding of oxidation state as well as short-range order structure, which may not be accessible from X-ray diffraction, without destroying batteries for measurements. Some in situ and ex

* Corresponding author. Tel.: +81 561 63 6126; fax: +81 561 63 6448.
E-mail address: nonaka@mosk.tytlabs.co.jp (T. Nonaka).

0378-7753/$ – see front matter © 2006 Elsevier B.V. All rights reserved.
doi:10.1016/j.jpowsour.2006.09.003

situ XAFS measurements on $LiNi_{1-x}Co_xO_2$ systems have been reported [10–17]. These investigations successfully elucidated the change in the electronic and atomic structure around Ni and Co during charge/discharge for fresh batteries. However, little has been known concerning such changes for the capacity faded batteries.

The purposes of this study are: (1) to clarify such electronic and structural change for a fresh (not deteriorated) battery, and (2) to compare the result for the fresh battery with those for batteries after cycle and aging tests. Such information will be of great significance in developing and utilizing batteries with this cathode material, and be one of the clues to solving the battery deterioration problem.

We have carried out not only in situ XAFS measurements using non-focused X-ray (conventional XAFS) but also those using X-ray microbeam with a focus size of about 2 μm (micro-XAFS). The former method provides bulk average data, whereas the latter method gives information from restricted areas on which X-ray microbeams are irradiated. In our practical use of Li-ion batteries, $LiNi_{0.8}Co_{0.15}Al_{0.05}O_2$ grains with the size of about 10–20 μm are used as cathodes. If the changes in Ni and Co oxidation states have a spatial distribution in each grain (e.g., the Ni valence at the center of a grain is higher than that at the grain boundary), our understanding on the cathode materials would require considerable modifications. Thus, in situ micro-XAFS has a potential to offer another insight into the electrochemical reaction proceeding in cathode particles, and can provide helpful information about the deterioration mechanism.

2. Experimental

2.1. Cells for in situ measurements

Fig. 1 shows a schematic view of the cell for in situ XAFS measurements. The cell consisted of a cathode, a Li foil anode, a 1 M $LiPF_6$ electrolyte dissolved in 1:1 (v/v) ethylene carbonate:diethyl carbonate (EC:DEC) solvent, a microporous polyethylene separator and 0.4 mm thick beryllium windows which enabled X-rays to penetrate through the cell. The cathode was a mixture of 80% (w/w) commercially available $LiNi_{0.8}Co_{0.15}Al_{0.05}O_2$, 10% conductive materials and 10% polyvinylidene fluoride (PVDF) binder. The cells were assembled in an argon-filled glove box. The cathode layers used in situ micro-XAFS measurements were controlled to be thin (less than 100 μm) enough to avoid the pile-up of cathode grains along the direction of X-ray microbeams. This ensured that each micro-XAFS spectrum reflected the information of a single grain.

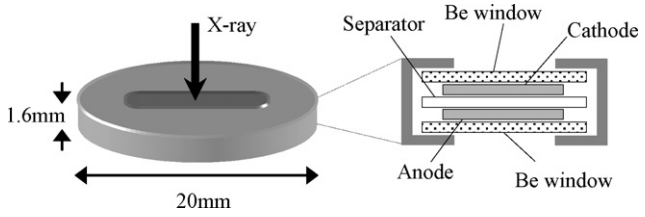

Fig. 1. Schematic view of coin cell used for in situ XAFS measurements.

Table 1
Conditions and capacities of in situ coin cells

Cell condition	Capacity[a] ($mAh\,g^{-1}$)
Cells for the in situ XAFS measurements	
Fresh: no charge/discharge cycle	140
Cycle test: 150 charge/discharge cycles at 60 °C	43
Aging test: stored at 60 °C for 15 days	133
Cells for the in situ micro-XAFS measurements	
Fresh: after 1 charge/discharge cycle	160
Cycle test: 100 charge/discharge cycles at 60 °C	112
Aging test: stored at 60 °C for 21 days	146

[a] Discharge capacity obtained at 3.2 V (see Fig. 2).

In the present study, we compared fresh cells (i.e., the cells that had been subjected to neither cycling nor aging tests) with the various tested cells. The conditions and discharge capacities of the cells are listed in Table 1. The galvanostatic curves of coin cells for in situ XAFS measurements are shown in Fig. 2. The cycle tests were carried out under constant current at a 0.56 $mA\,cm^{-2}$ between 4.18 and 3.2 V at 60 °C. The aging tests were performed by storing cells at 60 °C in air with the voltage held at 4.18 V (charged state).

2.2. In situ XAFS measurements and data analysis

The in situ XAFS measurements were performed on the bending magnet beamline BL16B2 of the SPring-8 (Hyogo, Japan). A pair of Si(1 1 1) crystals was used to monochromatize the incident X-rays. Harmonic contamination of the beam was rejected by means of a Rh-coated Si mirror. A beam size at the sample position was 1 mm × 3 mm. The X-ray intensities were monitored using ionization chambers filled with nitrogen gas for the incident beam and an argon–nitrogen mixture (25/75%) for the transmitted beam. The energy calibration of the monochromator was performed using a 6 μm thick Ni foil. XAFS scans covering both the Co and Ni K-edge spectra were recorded

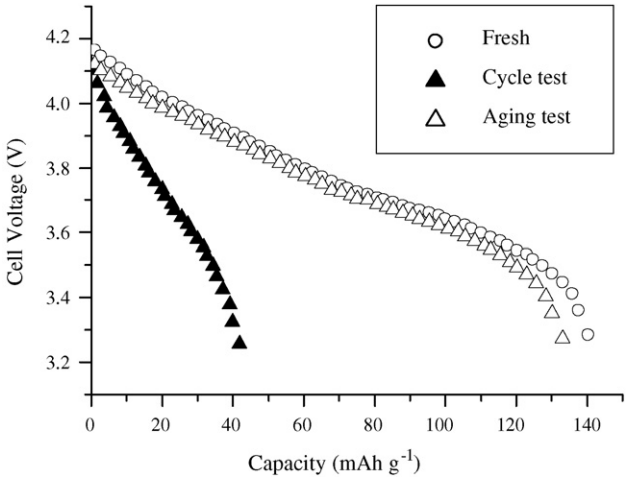

Fig. 2. Galvanostatic curves of coin cells for in situ XAFS during constant current discharge at a 0.113 $mA\,cm^{-2}$ (0.120 C rate). "Cell voltage" is the voltage measured between the cathode ($LiNi_{0.8}Co_{0.15}Al_{0.05}O_2$) and the anode (Li foil) during the discharge.

at several voltages of the cell. The charging between each XAFS scan was conducted in constant current–constant voltage mode (0.56 mA cm^{-2}). Each spectrum required 72 min for data acquisition.

The extended X-ray absorption fine structure (EXAFS) spectra were analyzed using conventional procedures, namely, pre- and post-edge background removal, normalization and Fourier filtering with a Hanning window, followed by curve-fitting. The software REX2000 (Rigaku Corp.) was employed for all computations. The phase shifts and back-scattering amplitudes used for the curve-fitting were calculated by the FEFF code (Version 8.2) [18].

2.3. In situ micro-XAFS measurements

The in situ micro-XAFS measurements were carried out on the insertion device beamline BL16XU of the SPring-8. The beamline is equipped with an optical system to generate X-ray microbeams using two elliptical Kirkpatrick–Baez (KB) mirrors [19]. The KB mirrors provide a focused beam with the size ranging from microns to sub-microns at the sample position. The full width at half maximum of the microbeam used in this study was about 2 μm. Fig. 3 illustrates the experimental setup for the in situ micro-XAFS measurements. A sample mounted on a high-precision two-dimensional moving stage is irradiated with X-ray microbeams. X-ray fluorescence and transmission maps can be obtained by scanning the sample with respect to microbeams. A silicon semiconductor detector (SSD) and an ionization chamber are employed to collect fluorescent and transmitted X-rays, respectively.

The experimental procedure was as follows. A discharged coin cell (3.0 V) was mounted on the sample stage; and then Ni and Co Kα fluorescence maps with a size of 100 μm × 100 μm were obtained at 9.0 keV. At several points in the fluorescence maps, Ni and Co K-edge X-ray absorption near edge structure (XANES) spectra were recorded in the transmission mode. Following XANES measurements for all points, the cell was charged to 4.2 V and XANES measurements were performed again. In order to minimize the radiation damage which may cause the change in Ni and Co valences, the XANES spectra at 4.2 V were collected at the points that had not been used for the measurements at 3.0 V.

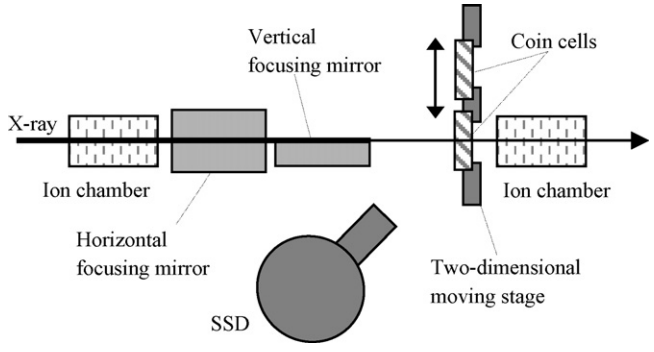

Fig. 3. Experimental setup for in situ micro-XAFS in the transmission mode (top view).

3. Results and discussion

3.1. In situ XAFS measurements

3.1.1. XANES

Fig. 4a shows Ni K-edge XANES spectra for $LiNi_{0.8}Co_{0.15}Al_{0.05}O_2$ in representative cell states. It can be apparently seen that, as cell voltage increases, the entire pattern shifts to higher energies rigidly with little change in the shape of the spectrum. This positive shift indicates that the average valence of Ni increases upon charging (lithium extraction). It is generally considered that the value of the energy at half-step height (where normalized absorbance = 0.5) can be used as a measure of oxidation state. Fig. 5a compares the energies at half-step height as a function of cell voltage for the fresh, cycle tested and aging tested cells. It is clearly seen that all the cells exhibit the edge shifts to higher energies upon charging in almost the same way, indicating that the cycle and aging tests do not greatly affect the change of Ni oxidation state upon charging. The slight deviation of the edge energy among these cells at the same cell voltages is probably due to the deviation of Li content in cathode materials. In order to estimate the Li content, one has to know the

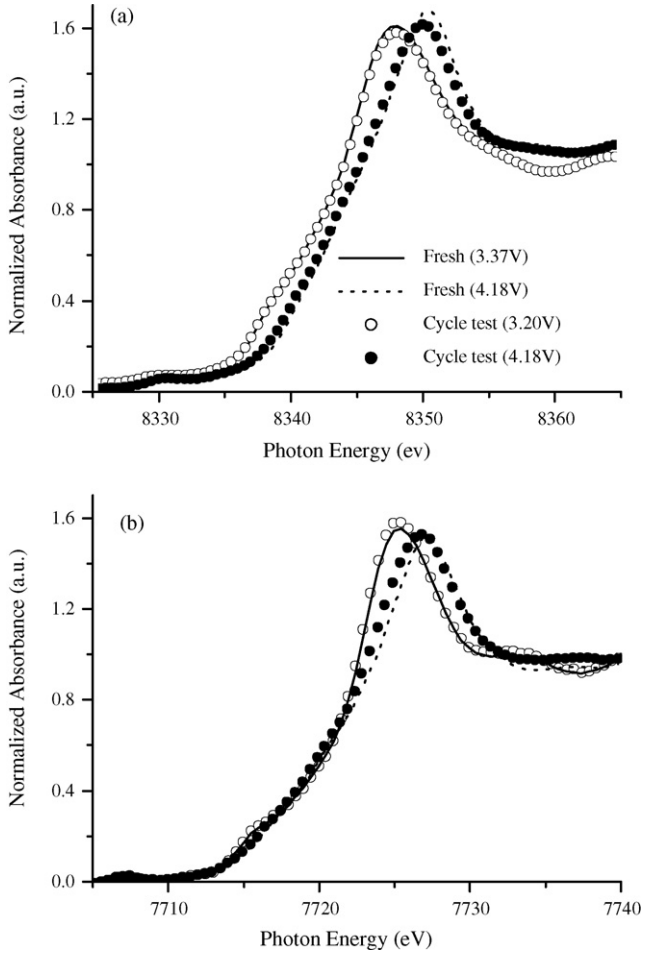

Fig. 4. Normalized XANES spectra for $LiNi_{0.8}Co_{0.15}Al_{0.05}O_2$ at: (a) Ni and (b) Co K-edge. "Cell voltage" is the open-circuit voltage measured after constant current–constant voltage charge (desired voltage, 0.316 mA cm^{-2} (0.336 C rate)).

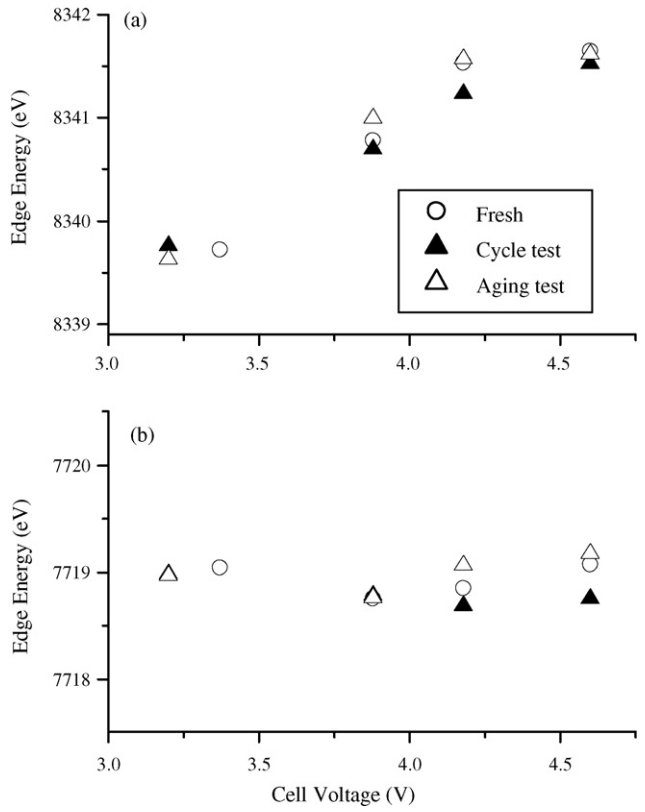

Fig. 5. Comparison of the edge energy measured at the half-step height of XANES spectra as a function of cell voltage at: (a) Ni and (b) Co K-edge.

total charge passed during cycling. In our in situ cells, it was impossible to measure the total current accurately due to the presence of self discharge and the accumulation of the slight errors in currents during cycle and aging tests. Fig. 6 shows the edge shift for the cycle tested cell relative to the analytical line proposed by O'Grady et al. [20]. They have reported systematic linear shifts in the edge energy (at half-step height) as a function of the Ni oxidation. It is evident that Ni atoms in the cycle tested cell are oxidized from Ni^{3+} to Ni^{4+} upon charging from 3.20 to 4.60 V. This trend of Ni oxidization is in good agreement

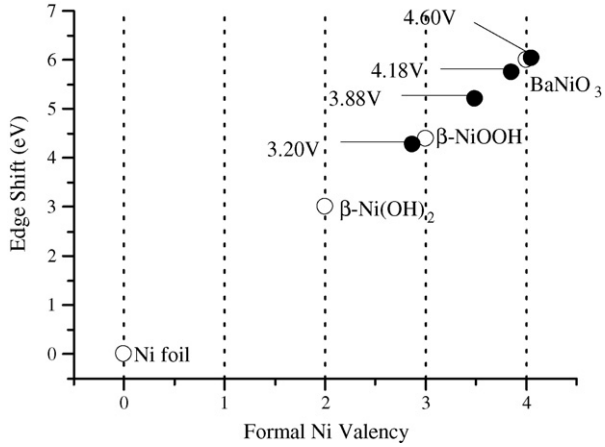

Fig. 6. Comparison of the Ni edge shift of the cycle tested cell during charging, with Ni reference standards.

with the findings of Balasubramanian et al. for $LiNi_{0.85}Co_{0.15}O_2$ [12].

Fig. 4b shows Co K-edge XANES spectra for $LiNi_{0.8}Co_{0.15}Al_{0.05}O_2$ in representative cell states. The rigid edge shift of the entire spectrum like Ni K-edge is not observed, whereas the shape of the spectrum changes upon charging particularly around the main peak. The shape and position of the main peak appear to change in the similar way as the Ni K-edge. Balasubramanian et al. have ascribed these changes to the local structure change of the host (Ni) lattice upon the removal of lithium [12]. We support this assertion since a clear correlation was found in another work between the main peak positions and the averaged Co–O bond distances obtained from the EXAFS analysis, which will be reported elsewhere. The edge energies at half-step height are compared in Fig. 5b. As opposed to the prominent shift observed at Ni K-edge, the Co edge can be seen unchanged upon charging. This suggests that Co hardly oxidizes and does not contribute to the charge compensation of $LiNi_{0.8}Co_{0.15}Al_{0.05}O_2$ upon lithium removal. As well as the Ni K-edge, the comparison of three cells shows that the Co oxidation state is not affected by the cycle and aging tests. (The slight differences depending on the cell condition are most likely to be due to the uncertainty of the edge energy caused by a relatively lower concentration of Co atom.)

3.1.2. EXAFS

Fourier-transforms of the Ni K-edge EXAFS spectra for representative cell states are shown in Fig. 7. The first peak at around 1.5 Å corresponds to Ni–O interaction and the second one at around 2.5 Å corresponds to Ni–M (M = Ni, Co) interaction. For both cells, it can be seen that the amplitude of Ni–O peak increases with charging. The smaller amplitude before charging is well understood by considering the local Jahn–Teller effect of NiO_6 octahedron expected for Ni^{3+} in a low-spin state. Nakai et al. have reported that distorted $Ni^{3+}O_6$ octahedral coordination,

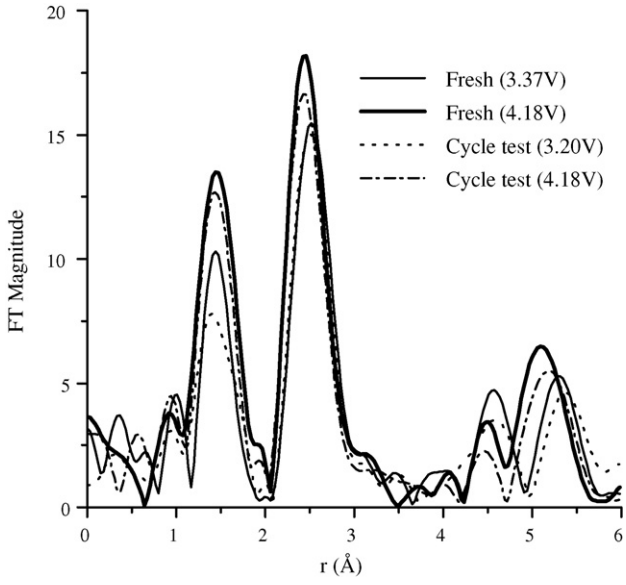

Fig. 7. Fourier-transforms of Ni K-edge EXAFS spectra for $LiNi_{0.8}Co_{0.15}Al_{0.05}O_2$.

including 4(shorter) + 2(longer) Ni–O bond distances, results in the apparent decrease in the amplitude of the Ni–O peak due to the interference of imaginary and real parts of the FT [10]. On the other hand, Ni^{4+} is not Jahn–Teller active ion; thus, oxidation of Ni^{3+} to Ni^{4+} results in the disappearance of the Jahn–Teller distortion and yields an increase in the amplitude of the Ni–O peak.

Quantitative analysis to obtain EXAFS structural parameters was performed by fitting the first two peaks in the FT. The following simple model was employed for the fitting procedure. The first Ni–O peak, which is actually composed of contributions from three subshells (two Ni^{3+}–Os and one Ni^{4+}–O), was fitted to one Ni–O shell. The second Ni–M (M = Ni, Co) peak was modeled as one Ni–Ni shell since the back-scattering amplitudes and phase shifts of neighboring elements (Co, Ni) are virtually indistinguishable. The coordination numbers of both shells were constrained to be six. The contribution to the EXAFS from lithium is too small and was not included in the fits.

In Fig. 8 are plotted bond distance and disorder (Debye–Waller factors) for Ni–O and Ni–M shells as a function of cell voltage. The average Ni–O bond distance (Fig. 8a) decreases with increasing cell voltage. This behavior is attributed to the conversion of Ni oxidation state from Ni^{3+} to Ni^{4+}. As described above the Ni^{3+}–O shell is composed of 4 shorter and 2 longer bonds, both of which are longer than the Ni^{4+}–O bond [12]. The behavior of the disorder for the Ni–O shell (Fig. 8b) is also understood by considering the change from Ni^{3+} to Ni^{4+}. The Jahn–Teller distorted $Ni^{3+}O_6$ octahedron results in larger Ni–O Debye–Waller factors. These findings for the Ni–O shell are completely consistent with the XANES results. The Ni–M bond distance (Fig. 8c) decreases upon charging, which is consistent with the shrinkage of *a* lattice parameter obtained by X-ray diffraction [9]. The disorder for the Ni–M shell (Fig. 8d) slightly decreases upon charging. This may be due to the ordering of Ni–M layers caused by the distinction of the Jahn–Teller distorted $Ni^{3+}O_6$ octahedron. As can be clearly seen in Fig. 8, all the structural parameters obtained do not exhibit the dependence on the extent of the capacity fading. Not shown here, such dependence was not found also in the structural parameters obtained from Co K-edge EXAFS spectra.

Our XANES and EXAFS results clearly show that, upon charging, the electronic and local structures of Ni and Co in $LiNi_{0.8}Co_{0.15}Al_{0.05}O_2$ change reversibly even after the capacity fading is induced by cycle and aging tests. Such structural reversibility is probably caused by the Co and Al substitution. According to the XANES data, Co ion is practically electrochemical inactive during the cycling process, which can stabilize the layered structure. Al-doping is also considered to have the similar stabilizing effect as Co-doping [8]. However, it should be noticed that these results obtained by Ni and Co K-edge XAFS in the transmission mode reflects the average bulk information

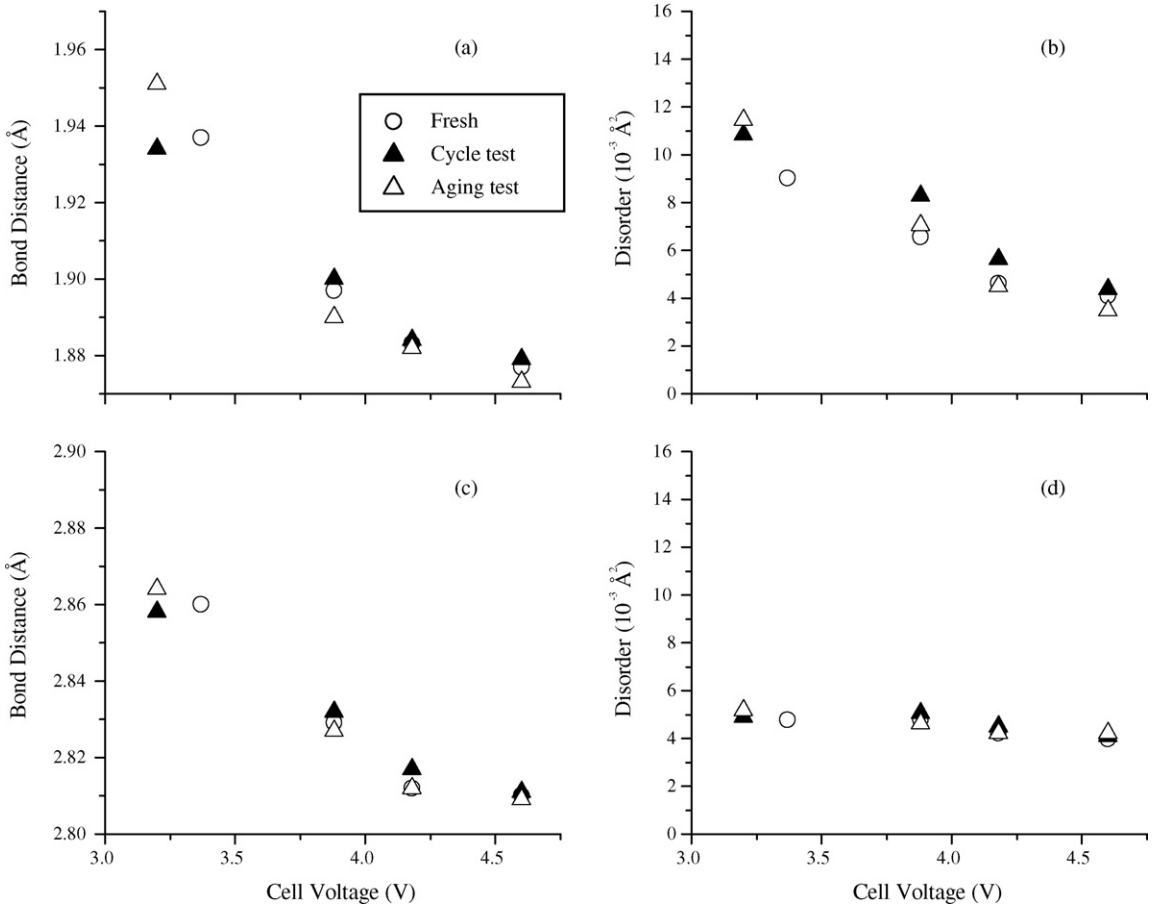

Fig. 8. Variations of structural parameters from the fitting to the first two peaks of the Ni K-edge FT: (a) average Ni–O bond distance, (b) disorder (Debye–Waller factor) for Ni–O shell, (c) Ni–M (M = Ni, Co) bond distance and (d) disorder for Ni–M shell.

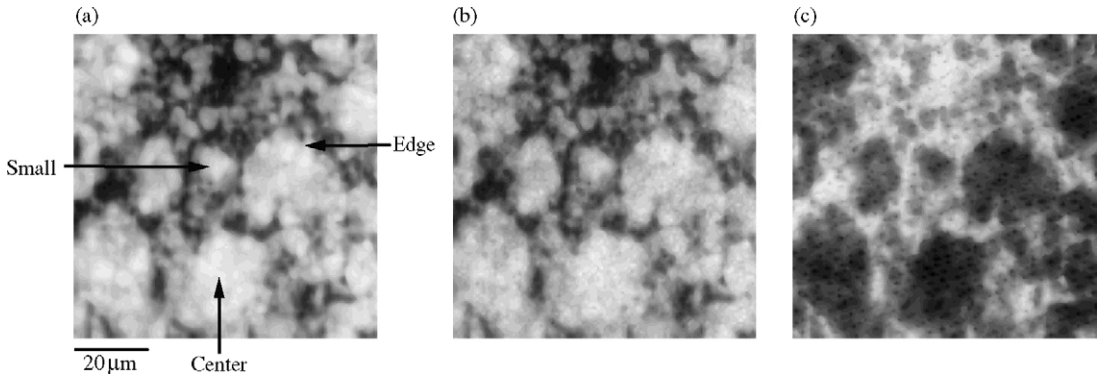

Fig. 9. 100 μm × 100 μm X-ray fluorescence map of: (a) Ni and (b) Co in $LiNi_{0.8}Co_{0.15}Al_{0.05}O_2$ (fresh cell). (c) Transmission X-ray map of $LiNi_{0.8}Co_{0.15}Al_{0.05}O_2$. The brightness is proportional to the X-ray intensity. Representative points where micro-XAFS spectra were recorded are indicated in (a).

about the cathode material. We cannot exclude the possibility that, by cycle and aging tests, slight changes are induced locally, e.g., only on the surface of the cathode material particles.

3.2. *In situ micro-XAFS measurements*

Fig. 9a and b shows 100 μm × 100 μm X-ray fluorescence map of: (a) Ni and (b) Co in $LiNi_{0.8}Co_{0.15}Al_{0.05}O_2$ of the fresh cell. Grains of cathode materials with the size of 10–20 μm (bright areas) are clearly observed in these fluorescence maps. The distribution of Co atoms appears to be completely identical to that of Ni atoms, indicating the uniform mixing of Ni and Co at least within the special resolution of the measurement (∼2 μm). The X-ray transmission map shown in Fig. 9c is seen to be the "negative image" of the Ni and Co fluorescence maps, which demonstrates that the thickness of the cathode is thin enough to prevent grains from piling up along the path of X-rays, as is expected. For the cycle tested cell and aging tested cell, the maps similar to those of the fresh cell were obtained and no distinct difference among these maps has been observed.

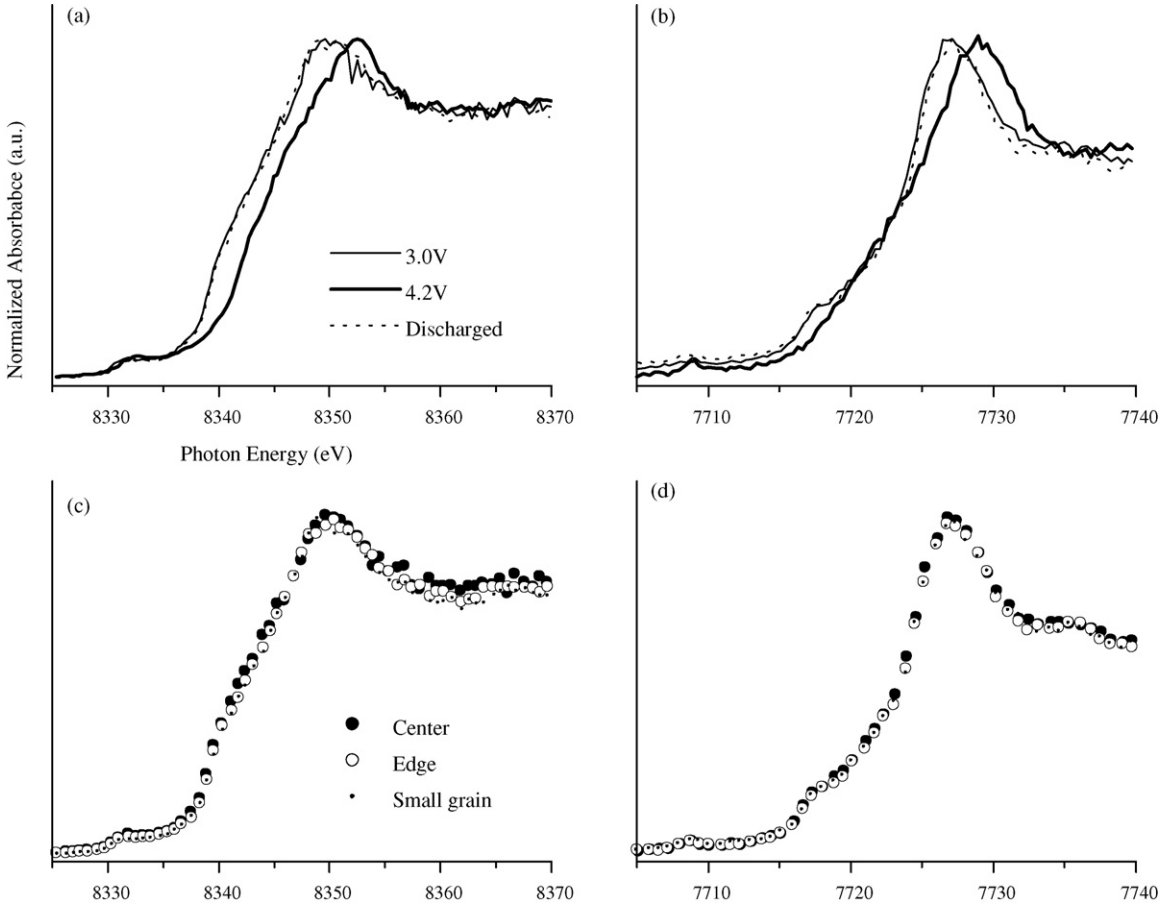

Fig. 10. Representative micro-XANES spectra recorded at edges of grains in the fresh cell at: (a) Ni and (b) Co K-edge. Position dependence of micro-XANES spectra at the (c) Ni and (d) Co K-edges.

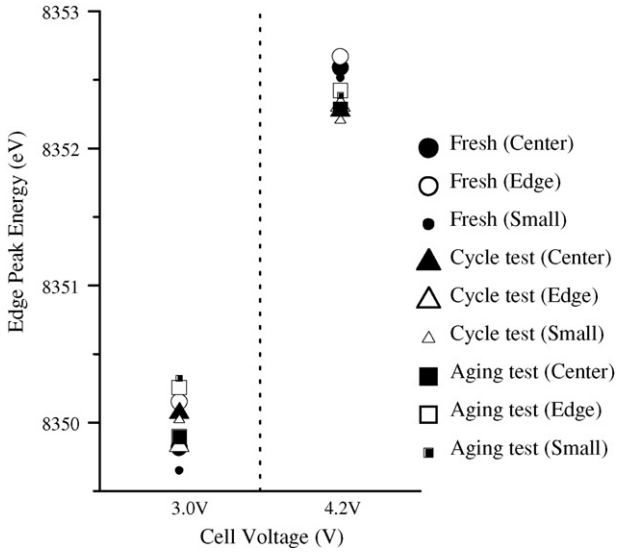

Fig. 11. Comparison of the Ni K-edge peak energies; dependences on measuring positions and on cell conditions.

Fig. 10a and b shows the representative: (a) Ni and (b) Co K-edge micro-XANES spectra recorded at the edge of a grain in the fresh cell. Although the signal-to-noise ratio is poorer, the basic features appear to be identical to those of the conventional XANES spectrum. The Ni absorption edge shifts to higher energies upon charging similarly to the conventional Ni K-edge XANES, and regains the original shape and position after discharging, indicating the conversion of Ni oxidation states between Ni^{3+} and Ni^{4+}. Fig. 10c and d compares: (c) Ni and (d) Co K-edge micro-XANES spectra recorded at different positions indicated in Fig. 9a: the center of a large grain (∼20 μm in diameter), the edge of a large grain and the center of a small grain (∼10 μm). It can be seen that the position dependences are not present in these spectra.

In order to investigate thoroughly the position dependence and the dependence on the extent of the capacity fading, Ni K-edge micro-XANES spectra were collected at over 30 points. A quantitative comparison was performed using the Ni K-edge main peak energy as a measure of Ni oxidation state. Fig. 11 compares the edge peak energies as a function of cell voltage. As can be seen, no apparent tendencies depending on the position or on the cell condition are found. This indicates the following facts: (1) upon charging Ni is oxidized homogeneously (within the special resolution of ∼2 μm) in a grain of $LiNi_{0.8}Co_{0.15}Al_{0.05}O_2$, (2) the Ni oxidation proceeds independently of the grain size and (3) these homogeneity of the Ni oxidation are maintained after the capacity fading is induced by cycle or aging tests. As well as the Ni K-edge, the change in the Co K-edge peak energy (not shown) does not have tendencies depending on the position or on the cell condition.

4. Conclusions

In situ XAFS and in situ micro-XAFS techniques have been applied to study $LiNi_{0.8}Co_{0.15}Al_{0.05}O_2$ cathode materials in Li-ion coin cells that showed various levels of capacity fade. The evolution of the electronic and local structure of Ni and Co during charge has been investigated. The conclusions of this study are as follows:

1. Ni and Co K-edge XANES show that the Ni oxidation state is converted from Ni^{3+} to Ni^{4+} upon charging, whereas the Co oxidation state hardly changes.
2. Ni K-edge EXAFS reveals that the Jahn–Teller distorted NiO_6 octahedron turns into the symmetric octahedron upon charging, which is consistent with the change in the Ni oxidation state.
3. Ni K-edge micro-XANES show that the oxidation of Ni proceeds homogeneously in a grain of $LiNi_{0.8}Co_{0.15}Al_{0.05}O_2$ within the special resolution of ∼2 μm, and proceeds independently of the grain size.
4. All the behaviors of Ni and Co observed in these experiments for the fresh cell remain unchanged after the capacity fade is induced by cycle tests or aging tests, which demonstrates the considerable stability of the $LiNi_{0.8}Co_{0.15}Al_{0.05}O_2$ cathode material. The results also suggest that proving methods with higher special resolution and/or with higher precision are necessary to explore the origin of the capacity fading and the increase in impedance.

Acknowledgements

The authors are grateful to T. Okamoto, Y. Takeuchi, Y. Itou, H. Matsuo, O. Hiruta and S. Kawauchi for their contributions to this work and would like to thank H. Tanida for the development of the software for XAFS measurements.

References

[1] J.M. Tarascon, M. Armand, Nature 414 (2001) 361.
[2] C. Delmas, M. Menetier, L. Fournes, Electrochim. Acta 45 (1999) 243.
[3] T. Ohzuku, A. Ueda, M. Nagayama, J. Electrochem. Soc. 140 (1993) 1862.
[4] C. Delmas, I. Saadoune, A. Rougier, J. Power Sources 44 (1993) 592.
[5] M.R. Palacin, D. Larcher, A. Audemer, N. Sac-Epee, G.G. Amatucci, J.M. Tarascon, J. Electrochem. Soc. 144 (1997) 4226.
[6] E. Levi, M.D. Levi, G. Salitra, D. Aurbach, R. Oesten, U. Heider, L. Heider, Solid State Ionics 126 (1999) 97.
[7] T. Ohzuku, A. Ueda, M. Kouguchi, J. Electrochem. Soc. 142 (1995) 4033.
[8] H. Cao, B. Xia, N. Xu, C. Zhang, J. Alloys Compd. 376 (2004) 282.
[9] Y. Itou, Y. Ukyo, J. Power Sources 146 (2005) 39.
[10] I. Nakai, K. Takahashi, Y. Shiraishi, T. Nakagome, F. Izumi, Y. Ishii, F. Nishikawa, T. Konishi, J. Power Sources 68 (1997) 536.
[11] A.N. Mansour, J. McBreen, C.A. Melnedres, J. Electrochem. Soc. 146 (1999) 2799.
[12] M. Balasubramanian, X. Sun, X.Q. Yang, J. McBreen, J. Electrochem. Soc. 147 (2000) 2903.
[13] K.K. Lee, K.B. Kim, J. Electrochem. Soc. 147 (2000) 1709.
[14] A.N. Mansour, X.Q. Yang, X. Sun, J. McBreen, L. Croguennec, C. Delmas, J. Electrochem. Soc. 147 (2000) 2104.
[15] M. Balasubramanian, X. Sun, X.Q. Yang, J. McBeen, J. Power Sources 92 (2001) 1.
[16] J.M. Rosolen, M. Abbateb, Solid State Ionics 139 (2001) 83.
[17] C.S. Johnson, A.J. Kropf, Electrochim. Acta 47 (2002) 3187.
[18] S.I. Zabinsky, J.J. Rehr, A. Ankudinov, R.R. Albers, M.J. Eller, Phys. Rev. B 52 (1995) 2995.
[19] M. Hasegawa, Y. Hirai, J. Appl. Phys. 90 (2001) 2792.
[20] W.E. O'Grady, K.I. Pandya, K.E. Swider, D.A. Corrigan, J. Electrochem. Soc. 143 (1996) 1613.